Journal of Applied Physics

RESEARCH ARTICLE | JULY 29 2010

Design and fabrication of microcavity-array superhydrophobic surfaces

M. C. Salvadori; M. Cattani; M. R. S. Oliveira; F. S. Teixeira; I. G. Brown

J. Appl. Phys. 108, 024908 (2010)
https://doi.org/10.1063/1.3466979

AIP Publishing

Design and fabrication of microcavity-array superhydrophobic surfaces

M. C. Salvadori,[1,a)] M. Cattani,[1] M. R. S. Oliveira,[2] F. S. Teixeira,[2] and I. G. Brown[3]
[1]*Institute of Physics, University of São Paulo, São Paulo, C.P. 66318, CEP 05315-970 São Paulo, Brazil*
[2]*Polytechnic School, University of São Paulo, Av. Prof. Luciano Gualberto, Travessa R, 158, CEP 05508-900 São Paulo, São Paulo, Brazil*
[3]*Lawrence Berkeley National Laboratory, Berkeley, California 94720, USA*

(Received 28 May 2010; accepted 22 June 2010; published online 29 July 2010)

We have modeled, fabricated, and characterized superhydrophobic surfaces with a morphology formed of periodic microstructures which are cavities. This surface morphology is the inverse of that generally reported in the literature when the surface is formed of pillars or protrusions, and has the advantage that when immersed in water the confined air inside the cavities tends to expel the invading water. This differs from the case of a surface morphology formed of pillars or protrusions, for which water can penetrate irreversibly among the microstructures, necessitating complete drying of the surface in order to again recover its superhydrophobic character. We have developed a theoretical model that allows calculation of the microcavity dimensions needed to obtain superhydrophobic surfaces composed of patterns of such microcavities, and that provides estimates of the advancing and receding contact angle as a function of microcavity parameters. The model predicts that the cavity aspect ratio (depth-to-diameter ratio) can be much less than unity, indicating that the microcavities do not need to be deep in order to obtain a surface with enhanced superhydrophobic character. Specific microcavity patterns have been fabricated in polydimethylsiloxane and characterized by scanning electron microscopy, atomic force microscopy, and contact angle measurements. The measured advancing and receding contact angles are in good agreement with the predictions of the model. © *2010 American Institute of Physics*. [doi:10.1063/1.3466979]

I. INTRODUCTION

The hydrophobicity of surfaces is important in an increasing variety of technological areas. Applications include microfluidics, microelectromechanical systems, self-cleaning surfaces, antifogging surfaces, resistance to oxidation, drag reduction, and more. In general, the wettability of a solid surface is governed by two factors. One is related to the solid and liquid chemistry of the material (low surface energy), and the other is the surface morphology.[1,2] Hydrophobic plant leaves have motivated researchers to reproduce the leaf morphology on material surfaces.[3–11] A typical example is shown in Fig. 1—the scanning electron microscope image of the surface of a lotus leaf.

Surface wetting is characterized by the contact angle made between a water droplet and the surface. The surface is said to be hydrophobic when the contact angle is greater than 90°, and surfaces with contact angle greater than 150° (up to 180°) are called superhydrophobic. Water droplets on smooth and flat hydrophobic surfaces do not usually have contact angles greater than 120°. Modification of the surface morphology can increase the contact angle without altering the surface chemistry. Following the lotus leaf morphology, technological approaches to fabricating superhydrophobic surfaces have generally been morphologies with pillars or protrusions.[12–17]

We have investigated the case for which the surface morphology consists of periodic microstructures which are cavities. This surface morphology is the inverse of that generally reported in the literature. The advantage of using a surface morphology formed of periodic microcavities is that when a surface of this morphology is immersed in water, the confined air inside the cavities tends to expel the invading water. This is quite distinct from the case of a surface morphology formed of pillars or protrusions, for which water can penetrate irreversibly among the microstructures, necessitating complete drying of the surface in order to again recover its superhydrophobic character. We point out that when our microcavity structure is fully immersed in water, a fraction of the trapped air will be dissolved in the water, progressively more so with pressure (immersion depth); the model described here does not include this feature. However, for the usual case of shallow immersion this effect is minimal and can be ignored.

We have developed a theoretical model that allows calculation of the microcavity dimensions needed to obtain su-

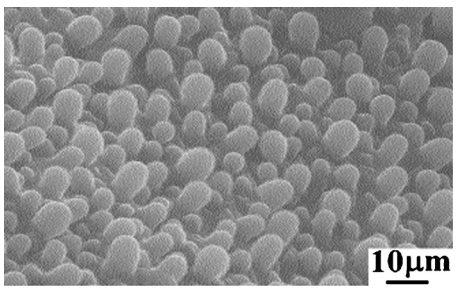

FIG. 1. Scanning electron micrograph of surface of lotus leaf.

[a)]Electronic mail: mcsalva@if.usp.br.

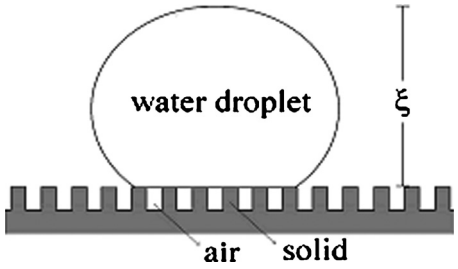

FIG. 2. Illustration of a water drop interfacing partially with the solid material and partially with the air confined in the cavities. ξ is the height of the droplet.

perhydrophobic surfaces composed of patterns of such microcavities, and that provides estimates of the advancing and receding contact angle as a function of microcavity parameters. A brief summary of our model has been presented in a prior publication;[18] here we describe the theoretical model in detail. Specific microcavity patterns as considered in the model were selected, and we have fabricated and characterized these surfaces by scanning electron microscopy (SEM), atomic force microscopy (AFM), and contact angle measurements.

II. THE MODEL

Our model conceptualizes a surface made of a solid material upon which microcavities are fabricated. When water is deposited on this surface, the cavities continue to confine air. Thus the surface water interfaces partially with the solid material and partially with the air confined in the microcavities as illustrated in Fig. 2. In order to calculate the final contact angles for these surfaces, the Cassie–Baxter law[19] is used: the cosine of the contact angle for a drop deposited on a heterogeneous surface is given by the average of the cosines of the different contact angles, weighted by the surface fractions of the heterogeneities. In the particular case where the surface is composed of a solid material (presenting contact angle θ) and air (confined in the cavities, and having contact angle 180°) the Cassie–Baxter law is given by the equation

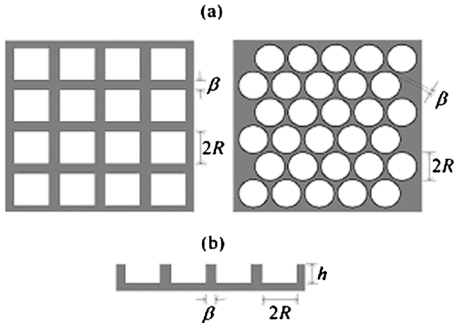

FIG. 3. (a) Top view of the two different cavity geometries used; (b) cross section of the cavity geometry for both cases. The parameters R, h, and β define completely the surface morphology.

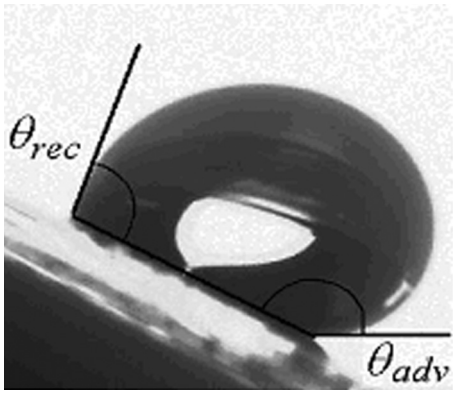

FIG. 4. Advancing and receding contact angles for a droplet which is just moving on an inclined surface.

$$\cos\,\theta^* = \phi_S \cos\,\theta + (1-\phi_S)(-1), \tag{1}$$

where θ^* is the contact angle of the heterogeneous surface, ϕ_S is the fractional surface area of the solid material, and (-1) is the cosine of 180°.

We consider two possible geometries: cavities with parallelepiped geometry and cavities with cylindrical geometry, as illustrated in Fig. 3. The parameters R, h, and β define completely the surface morphology. We assume that the solid material used for the surface fabrication has an advancing contact angle θ_{adv} greater then 90°, and a receding contact angle θ_{rec} less than 90°, as is common even for hydrophobic materials. [A droplet on an inclined surface sags toward the lower side, and the contact angle on the lower side is greater than that on the upper side. When the angle of tilt is such that the droplet just begins to move, these contact angles are called the advancing and receding contact angles (Fig. 4).]

The profile expected for the base of a water droplet deposited on the proposed surface is illustrated in Fig. 5(a). The pressure P_a applied on the water/air interface by the water can be written as

$$P_a = \rho g \xi + P_0, \tag{2}$$

where ρ is the water density, g the acceleration due to gravity, ξ the height of the water column to which the surface is

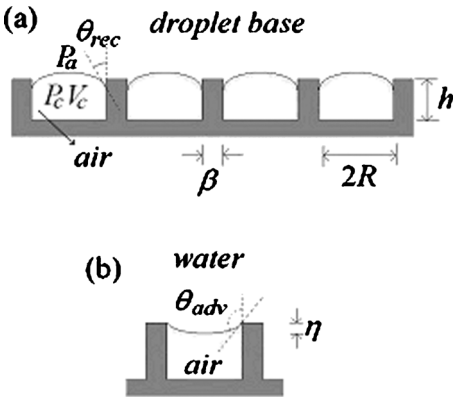

FIG. 5. (a) Expected profile for the base of a water drop deposited on the proposed surface fabricated from a solid material with receding contact angle θ_{rec} less than 90°. P_a is the pressure applied by the water at the water/air interface, and P_c and V_c are the pressure and volume, respectively, of the air confined in a cavity. (b) Expected profile for the base of a water drop when the water is intruding into the cavity.

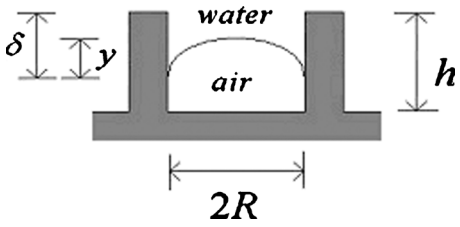

FIG. 6. Illustration of a cavity partially invaded by water, defining the parameters δ and y; δ is the maximum invasion distance.

subjected, and P_0 the atmospheric pressure. The pressure P_c and the volume V_c of the confined air in each cavity can be related to the initial pressure P_0 and volume V_i (before the drop completes deposition on the surface or before the surface is immersed in water), by the equation

$$P_c V_c = P_0 V_i. \tag{3}$$

Water tends to enter the cavities by capillarity, increasing the pressure P_c until reaching equilibrium. The pressure difference ΔP established inside a capillary of radius r is given quite generally by[20]

$$\Delta P = \frac{2\gamma \cos\theta}{r}, \tag{4}$$

where θ is the contact angle between the water and the solid surface in air and γ is the water surface tension. In this way, considering the water/air interface at the drop base in each cavity as a convex spherical cap in a cylindrical cavity or as a convex spherical cap inscribed in a square for parallelepiped cavities, we have

$$P_c - P_a = \frac{2\gamma \cos\theta}{R}. \tag{5}$$

Now we determine the pressure P_c inside each cavity. From Eq. (3) we have $P_c = P_0 V_i / V_c$, where V_i is the initial volume of the air confined in the cavity at atmospheric pressure P_0, and V_c is the volume of air at pressure P_c. Note that $V_i < V_0$, where V_0 is the geometric volume of the cavity. For cylindrical cavities

$$V_{0c} = \pi R^2 h = c_c R^2 h, \tag{6}$$

where $c_c = \pi$, and for parallelepiped cavities

$$V_{0p} = 4R^2 h = c_p R^2 h, \tag{7}$$

where $c_p = 4$. To determine V_i we need to consider the process of the water advancing over the cavity, where part of the cavity is invaded by a concave spherical cap as illustrated in Fig. 5(b). This is because the contact angle to be considered in this case is the advancing contact angle θ_{adv}. Thus

$$V_i = V_0 - V_{cap}, \tag{8}$$

where V_{cap} is the volume of the concave spherical cap [see Fig. 5(b)]. The volume V_c can be calculated by considering the parameters δ as defined in Fig. 6, and we obtain

$$V_c = V_0\left(1 - \frac{\delta}{h}\right) + V_{cap}^*, \tag{9}$$

where V_{cap}^* is the volume of the convex spherical cap (see Fig. 6).

Substituting Eqs. (8) and (9) into Eq. (3) results in

$$P_c = P_0 \frac{V_0 - V_{cap}}{V_0(1 - \delta/h) + V_{cap}^*} = \frac{1 - V_{cap}/V_0}{V_0(1 - \delta/h) + V_{cap}^*/V_0}, \tag{10}$$

where $V_{cap} = \pi\eta(3R^2 + \eta^2)/6$ with $\eta = R(1 - \sin\theta_{adv})/-\cos\theta_{adv}$ [η is defined in Fig. 5(b)] and $V_{cap}^* = \pi y(3R^2 + y^2)/6$ with $y = R(1 - \sin\theta_{rec})/\cos\theta_{rec}$ (y is defined in Fig. 6), or

$$\frac{V_{cap}}{V_0} = -\frac{R}{h} f(\theta_{adv}) \tag{11}$$

and

$$\frac{V_{cap}^*}{V_0} = \frac{R}{h} f(\theta_{rec}), \tag{12}$$

where

$$f(\theta) = \frac{\pi}{6c} \frac{1 - \sin\theta}{\cos\theta}\left[3 + \frac{(1 - \sin\theta)^2}{(\cos\theta)^2}\right]. \tag{13}$$

Substituting Eqs. (11) and (12) into Eq. (10) we obtain

$$P_c = P_0 \frac{1 + \frac{R}{h} f(\theta_{adv})}{1 - \frac{\delta}{h} + \frac{R}{h} f(\theta_{rec})}, \tag{14}$$

and substituting Eqs. (2) and (14) into Eq. (5) we obtain finally

$$P_0\left[\frac{1 + \frac{R}{h} f(\theta_{adv})}{1 - \alpha + \frac{R}{h} f(\theta_{rec})} - 1\right] = \rho g \xi + \frac{2\gamma \cos\theta_{rec}}{R}, \tag{15}$$

where, to summarize the parameters used, P_0 is the atmospheric pressure, ρ the water density, g the acceleration due to gravity, ξ the height of the water column to which the surface is subjected or the height of the water droplet (see Fig. 2), R the radius of a cylindrical microcavity or half the length of the side of a square microcavity, γ the water surface tension, $\alpha = \delta/h$, the fractional vertical intrusion of water into a cavity as shown in Fig. 6, and obeys the condition $\alpha < 1$, and $f(\theta)$ is given by Eq. (13).

Equation (15) allows calculation of the cavity depth h as a function of the parameter R for a given fraction α of water penetration into the cavity. Figure 7 shows a plot of the cavity depth h as a function of R for $\alpha = 0.25$ and $\xi = 5$ mm, for the case when the surface is fabricated from PDMS (polydimethylsiloxane) with $\theta_{adv} = 119°$ and $\theta_{rec} = 86°$. Thus one can predict that a drop 5 mm in height will penetrate 25% of the cavity depth; in this case the cavity aspect ratio ($h/2R$) is less than unity for $R > 0.5$ μm, indicating that the microcavities do not need to be deep in order to obtain a surface with enhanced superhydrophobic character.

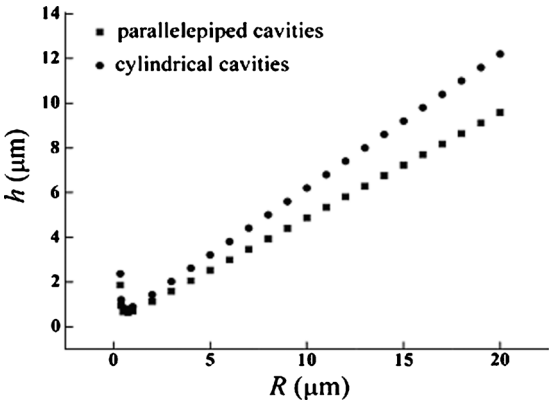

FIG. 7. Cavity depth h as a function of R (radius of a cylindrical cavity or half the length of the side of a square cavity), from Eq. (15) with $\alpha=0.25$, $\theta_{adv}=119°$, $\theta_{rec}=86°$, and $\xi=5$ mm.

To calculate the final contact angles θ^*_{adv} and θ^*_{rec} of the fabricated surface, we use the Cassie–Baxter law given by Eq. (1), where θ is the characteristic contact angle (θ_{adv} or θ_{rec}) of the solid material used to fabricate the surface and ϕ_S is the fraction of the surface area over which the drop maintains contact with the solid material. To calculate the advancing contact angle θ^*_{adv}, we estimate the fraction of surface area for which the drop is in contact with the solid material as illustrated in Fig. 8.

In this way we obtain,

$$\phi^p_{adv} = \frac{\beta(4R+\beta)}{(2R+\beta)^2} \text{(for parallelepiped cavities)}, \tag{16}$$

and

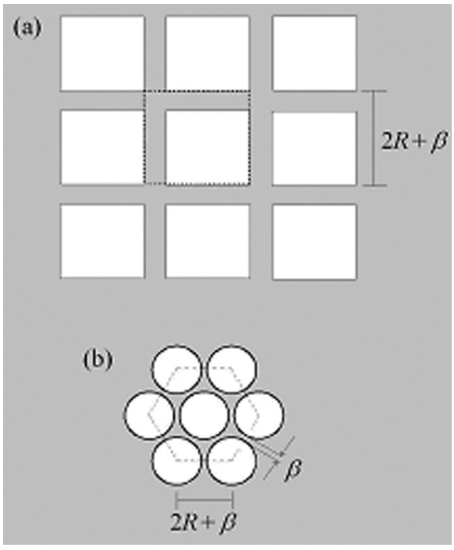

FIG. 8. Top view of the surface morphology to determine the fraction of the surface area over which the drop is in contact with the solid material. (a) The square delimited by dashed lines defines an elemental area that can reproduce the entire surface, for cavities with parallelepiped geometry. (b) The hexagon delimited by dashed lines defines an elemental area that can reproduce the entire surface, for cylindrical cavities.

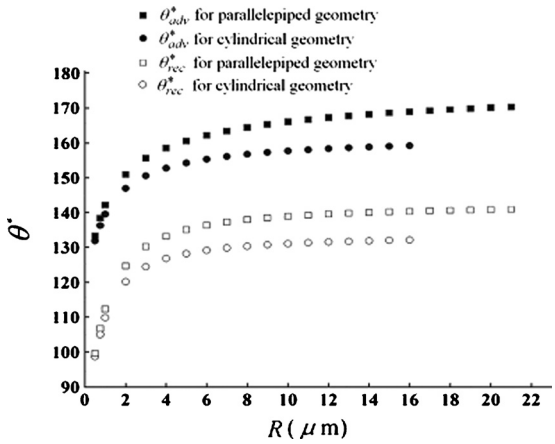

FIG. 9. Advancing θ^*_{adv} and receding θ^*_{rec} contact angles as a function of R for both cavity geometries, from Eqs. (20) and (21) with $\theta_{adv}=119°$, $\theta_{rec}=86°$, $\beta=0.6$ μm, $h=2.5$ μm, and α was calculated using Eq. (15).

$$\phi^c_{adv} = \frac{(2R+\beta)^2 - \frac{2\pi}{\sqrt{3}}R^2}{(2R+\beta)^2} \text{ (for cylindrical cavities)}. \tag{17}$$

To calculate the receding contact angle θ^*_{rec} of the surface, we take into account that the water invasion into the cavities increases the fraction of surface area over which the drop is in contact with the solid material. For these conditions we have

$$\phi^p_{rec} = \frac{\beta(4R+\beta)+8R\alpha h}{(2R+\beta)^2+8R\alpha h} \text{ (for parallelepiped cavities)} \tag{18}$$

and

$$\phi^c_{rec} = 1 - R^2\left[\frac{\sqrt{3}}{2\pi}(2R+\beta)^2 + 2R\alpha h\right]^{-1} \text{ (for cylindrical cavities)}. \tag{19}$$

Then finally, using Eq. (1), the contact angles of the surface are given by

$$\cos\theta^*_{adv} = \phi_{adv}\cos\theta_{adv} + (1-\phi_{adv})(-1) \tag{20}$$

and

$$\cos\theta^*_{rec} = \phi_{rec}\cos\theta_{rec} + (1-\phi_{rec})(-1). \tag{21}$$

Plots of the calculated advancing θ^*_{adv} and receding θ^*_{rec} contact angles are shown in Fig. 9 as a function of R, for both cavity geometries considered (parallelepiped and cylindrical). Here we assumed $\theta_{adv}=119°$, $\theta_{rec}=86°$, $h=2.5$ μm, α was calculated using Eq. (15), and the "wall thickness" β as defined in Fig. 3 was $\beta=0.6$ μm. Note that for $h=2.5$ μm we have a maximum value of R, since α must be less than unity. The maximum R is about 21 μm for parallelepiped cavities and about 16 μm for cylindrical cavities.

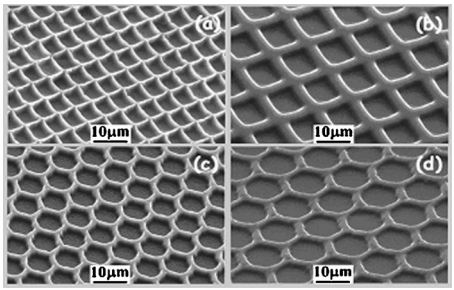

FIG. 10. Scanning electron micrographs of the four lithographed samples; (a) and (b) show parallelepiped cavities and (c) and (d) cylindrical cavities.

III. THE MICROFABRICATED SURFACES

We describe now four microfabricated surfaces based on the above model, two with parallelepiped cavity geometry and two with cylindrical cavity geometry. The advancing and receding contact angles were measured and compared with the predictions of the theory.

The material used for the surface fabrication was PDMS (polydimethylsiloxane). Silicon substrates (pieces of wafer) were cleaned, and baked at 200 °C for 30 min to remove residual humidity. The electron resist SU-8 (SU-8 2002, MicroChem Corp.) was then deposited on the silicon using a spin coater. The samples were baked again at 65 °C for 1 min and 95 °C for 2 min to evaporate the polymer solvent. Samples were then transferred to a scanning electron microscope, JEOL model JSM-6460 LV, equipped with an e-beam nanolithography system (nanometer pattern generation system) and the desired pattern transferred to the SU-8 surface. The samples were immersed in a developing solution, generating the desired microcavities on the surface. The total area lithographed on each surface was 9×9 mm^2. Two PDMS replicas were obtained from each lithographed sample, first a negative replica (presenting periodic protrusions) and also a positive replica (presenting cavities). The PDMS replicas were imaged by SEM and AFM. Contact angle measurements were made using a CAM 200 system (from KSV Instruments). Figure 10 shows scanning electron micrographs of the four SU-8 lithographed samples. The samples were replicated in PDMS and the advancing θ^*_{adv} and receding θ^*_{rec} contact angles measured.

Contact angle measurements were performed by a dynamic sessile drop method. In this method the surface is tilted until the droplet just starts to move on the surface, at which point the advancing and receding contact angles are measured from an image of the droplet. Figure 11 shows droplet images for each of the four PDMS microcavity samples and for a droplet on a flat PDMS surface. The critical surface tilt angle depends on θ_{adv} and θ_{rec}, the liquid/vapor surface tension and the droplet size, and the surface tilts shown in the figure are the critical tilt angles. The droplet size was about 22 μL.

The contact angle results are summarized in Table I. The measured advancing contact angles were between 141° and 153° (for different microcavity geometries as shown in the table), and the receding contact angles between 98° and 107°, in good agreement with the calculated values.

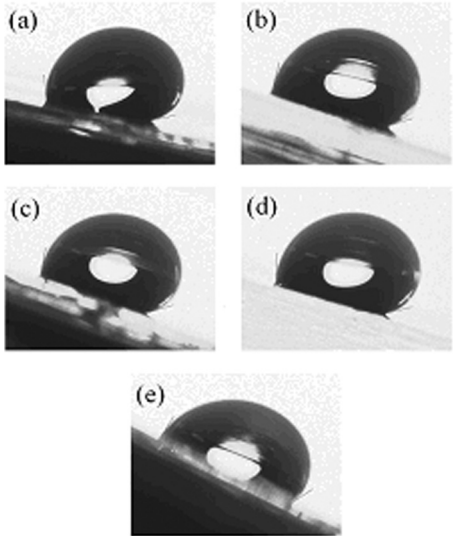

FIG. 11. Images of droplets on each of the four PDMS samples [(a) and (b) refer to the parallelepiped cavities with $R=3.3$ μm and $R=4.8$ μm, respectively; (c) and (d) refer to the cylindrical cavities with $R=3.4$ μm and $R=5.2$ μm, respectively], and (e) on a flat PDMS surface (no microstructure). The surfaces are tilted at an angle such that the droplet just begins to move.

IV. DISCUSSION AND SUMMARY

We have developed a model for designing superhydrophobic surfaces with morphology formed of an extended array of microcavities. The advantage of this morphology is that even when the surface is fully immersed in (shallow) water, the confined air inside the cavities tends to expel the invading water, whereas for the more usual case of a surface morphology formed of microprotrusions water can penetrate irreversibly among the microstructures. The microprotrusion morphology thus necessitates complete drying of the surface in order to recover its superhydrophobic character, while the microcavity morphology retains its superhydrophobicity after full immersion (in shallow water).

The model allows calculation of the microcavity dimensions needed to obtain superhydrophobic surfaces and provides estimates of the advancing and receding contact angles as a function of microcavity parameters. We have considered two possible specific geometries: cavities with parallelepiped geometry and cavities with cylindrical geometry. We assume that the solid material used for the surface fabrication has an advancing contact angle θ_{adv} greater then 90°, and a receding contact angle θ_{rec} less than 90°, as is common even for hydrophobic materials. The model considers the different contributions to the pressure equilibrium on the water interface with the air confined in a microcavity, including the pressure due to the water column to which the surface is subjected (ξ), the atmospheric pressure (P_0), the pressure due to the capillarity effect in the cavity, and the pressure of the confined air in each cavity (P_c). The model correlates ξ, R (radius of a cylindrical microcavity or half the length of the side of a square microcavity), $\alpha=\delta/h$ (fractional vertical intrusion of water into a cavity), P_0, ρ (water density), g

TABLE I. Summary of results: SEM image of the relevant surface; microcavity dimensions R, β, and h as defined in Fig. 3; advancing θ^*_{adv} and receding θ^*_{rec} contact angles, comparing calculated and measured values.

				Advancing contact angle		Receding contact angle	
SEM of surface	R μm	β μm	h μm	θ^*_{calc} *adv*	θ^*_{meas} *adv*	θ^*_{calc} *rec*	θ^*_{meas} *rec*
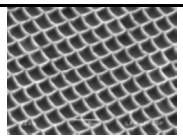	3.3	0.7	2.1	155°	153°	130°	107°
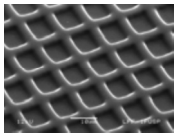	4.8	2.9	2.1	142°	141°	118°	98°
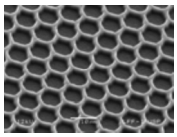	3.4	2.5	2.1	137°	141°	112°	102°
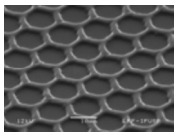	5.2	2.4	1.4	141°	147°	119°	106°

(acceleration due to gravity), γ (water surface tension), θ_{adv} (advancing contact angle), and θ_{rec} (receding contact angle) of the solid material used for the surface fabrication. This relationship, Eq. (15), allows calculation of the cavity depth h as a function of R for given fraction α of water penetration into the cavity. An important prediction of the model is that the cavity aspect ratio $(h/2R)$ can be much less than unity, indicating that the microcavities do not need to be deep in order to obtain a surface with enhanced superhydrophobic character. To calculate the final advancing and receding contact angles of the fabricated surface, we applied the Cassie–Baxter law, using the characteristic contact angle (θ_{adv} or θ_{rec}) of the solid material used to fabricate the surface and the fraction of the surface area over which the drop maintains contact with the solid material (ϕ_S).

Four different surfaces based on the model were fabricated in PDMS, two with parallelepiped cavity geometry and two with cylindrical cavity geometry. The surfaces were characterized by SEM and AFM, and the advancing and receding contact angles were measured and compared with the predictions of the theory, showing good agreement. The theory described here allows design of hydrophobic surfaces for the case not only for droplets resting on the surface at atmospheric pressure but also for the case when the surface is fully submerged (in water not too deep).

ACKNOWLEDGMENTS

This work was supported by the Fundação de Amparo a Pesquisa do Estado de São Paulo (FAPESP) and the Conselho Nacional de Desenvolvimento Científico e Tecnológico (CNPq), Brazil.

[1] R. W. Wenzel, Ind. Eng. Chem. **28**, 988 (1936).
[2] R. D. Hazlett, J. Colloid Interface Sci. **137**, 527 (1990).
[3] W. Barthlott and C. Neinhuis, Planta **202**, 1 (1997).
[4] P. Wagner, R. Fürstner, W. Barthlott, and C. Neinhuis, J. Exp. Bot. **54**, 1295 (2003).
[5] A. Marmur, Langmuir **20**, 3517 (2004).
[6] T. Sun, L. Feng, X. Gao, and L. Jiang, Acc. Chem. Res. **38**, 644 (2005).
[7] L. Zhai, M. C. Berg, F. C. Cebeci, Y. Kim, J. M. Milwid, M. F. Rubner, and R. E. Cohen, Nano Lett. **6**, 1213 (2006).
[8] S. M. Lee and T. H. Kwon, Nanotechnology **17**, 3189 (2006).
[9] S. Wang, Y. Zhu, F. Xia, Y. J. Xi, N. Wang, L. Feng, and L. Jiang, Carbon **44**, 1848 (2006).
[10] B. Bhushan and Y. C. Jung, Nanotechnology **17**, 2758 (2006).
[11] L. Gao and T. J. McCarthy, Langmuir **22**, 5998 (2006).
[12] D. Öner and T. J. McCarthy, Langmuir **16**, 7777 (2000).
[13] R. Blossey, Nature Mater. **2**, 301 (2003).
[14] N. J. Shirtcliffe, S. Aqil, C. Evans, G. McHale, M. I. Newton, C. C. Perry, and P. Roach, J. Micromech. Microeng. **14**, 1384 (2004).
[15] H. Yabu, M. Takebayashi, M. Tanaka, and M. Shimomura, Langmuir **21**, 3235 (2005).
[16] A. Shastry, M. J. Case, and K. F. Böhringer, Langmuir **22**, 6161 (2006).
[17] Y. K. Jung and B. J. Bhushan, J. Microsc. **229**, 127 (2008).
[18] M. C. Salvadori, M. Cattani, M. R. S. Oliveira, F. S. Teixeira, and I. G. Brown, Appl. Phys. Lett. **96**, 074101 (2010).
[19] A. B. D. Cassie and S. Baxter, Nature (London) **155**, 21 (1945).
[20] F. W. Sears, *Principles of Physics I: Mechanics, Heat, and Sound* (Addison-Wesley, Cambridge, MA, 1970).